JOURNAL OF SOLID STATE CHEMISTRY 107, 401–412 (1993)

Structure and Magnetism of Anhydrous $FeAsO_4$: Inter- vs Intradimer Magnetic Exchange Interactions

W. M. REIFF* AND M. J. KWIECIEN†

Department of Chemistry, Northeastern University, Boston, Massachusetts 02115

R. J. B. JAKEMAN AND A. K. CHEETHAM*,‡

Chemical Crystallography Laboratory, University of Oxford, Oxford, OX1 3PD, United Kingdom

AND C. C. TORARDI*

DuPont Central Research and Development, Experimental Station, Wilmington, Delaware 19880-0356

Received December 7, 1992; accepted March 22, 1993

The structure of anhydrous $FeAsO_4$ has been refined from single crystal X-ray diffraction data. It displays a unique network of pairs of edge-sharing FeO_5 units interconnected by AsO_4 tetrahedra. Magnetic susceptibility measurements reveal pairwise antiferromagnetic exchange ($T_{\chi max} \sim 83$ K) while low-temperature Mössbauer spectra show three-dimensional ordering at ~67.5 K. An effective internal hyperfine field of 517 kG was calculated from the Zeeman-split Mössbauer spectrum at 4.2 K. These magnetic phenomena are discussed in terms of interdimer and intradimer magnetic exchange interactions. The intradimer exchange constant ($J \sim -23$ cm^{-1}) was estimated from the susceptibility data using the Heisenberg–Dirac–Van Vleck equation. In the range 290 ~ 190 K, the magnetic susceptibility obeys the Curie–Weiss expression ($\theta = -231$ K, $\mu = 5.90$ B.M.), suggesting dominant antiferromagnetic exchange interactions. The temperature and field dependence of the molar susceptibility also give evidence of a further magnetic transition at ~4.5 K.

Introduction

In recent years, the combination of Mössbauer spectroscopy, magnetic susceptibility, and powder neutron diffraction measurements has been successfully used to determine the complex relationship between crystalline structure and magnetic structure for three-dimensional network materials (*1–4*). Ferric phosphate and ferric sulfate are two such network materials which show three-dimensional magnetic order at low temperatures and for which detailed magnetostructural correlations have been determined (*3, 4*). Iron (III) is tetrahedrally coordinated in the former complex and octahedrally coordinated in the latter. Prior to the structure determination of the title compound (vide infra), among the few known examples of five-coordinate high-spin iron (III) in an oxyanion network system were Fe_3PO_7 (*5*) and $Fe_4(PO_4)_2O$ (*6*). In the present study, a new example of a high-spin, five-coordinate, Fe(III) network system is investigated. A comparison of the $FeAsO_4$ system with Fe_3PO_7 and with other Fe(III)-oxyanion systems provides valuable

* To whom correspondence should be addressed.

† Current address: Gillette Corporation, Boston, MA 02127.

‡ Current address: Materials Department, University of California, Santa Barbara, CA 93106.

0022-4596/93 $5.00

insight into the relationship between the coordination geometry and the magnetic properties of network compounds for iron (III) in four-, five-, and six-coordination. Of the iron (III) salts based on tetrahedral oxyanions and known to undergo magnetic phase transitions (e.g., $FePO_4$, $Fe_2(SO_4)_3$, $Fe_2(MoO_4)_3$ (*3, 4, 1*)), ferric phosphate is particularly interesting since, in addition to undergoing a transition to three-dimensional antiferromagnetic order at 24 K, it also appears to undergo a novel phase transition at 17 K in which the direction of the ordered electronic spin rotates within the antiferromagnetic structure (*3*). Such spin reorientation transitions are not unprecedented. α-Fe_2O_3, for example, undergoes a similar spin reorientation at 260 K, the well known Morin transition. However, unlike $FePO_4$, this reorientation accompanies a change in the magnetic character of the material from antiferromagnetism <260 K to weakly ferromagnetic between 260 and 956 K (*7*). We were encouraged by the interesting magnetic behavior of $FePO_4$ to conduct a detailed study of the magnetism and Mössbauer spectroscopy of the stoichiometrically similar $FeAsO_4$, although, strictly speaking, these materials are not directly comparable, as evidenced by the different structure reported herein.

Although the preparation of $FeAsO_4$ was first reported by Shafer *et al.* (*8*) in 1956, it was surprising to find at the outset of this work that neither the structure nor low-temperature Mössbauer spectroscopy data for anhydrous $FeAsO_4$ has been reported. Our objective in the present study, therefore, was to magnetically characterize anhydrous iron (III) arsenate down to 4.2 K and ultimately to correlate, if possible, our findings with the single-crystal X-ray structure refinement of the present investigation. In the meantime, determination of the structure of $FeAsO_4$ for a *polycrystalline powder sample*, using a neutron diffraction spallation source, has been accomplished and published elsewhere (*9*). The results of the latter investigation agree in essentially all details with those of the single-crystal X-ray diffraction study reported herein.

2. Experimental

2.1. Sample Preparation

Powder samples of anydrous $FeAsO_4$ were obtained by first preparing $FeAsO_4 \cdot 2H_2O$ (mineral name scorodite), then heating the dihydrate in air in an alumina crucible at 800°C for 24 hr. No impurity lines were observed in the X-ray powder diffraction pattern of the anydrous compound, and all diffraction peaks fit the monoclinic unit cell described by D'Yvoire (*10*). The $FeAsO_4 \cdot 2H_2O$ precursor was synthesized by reaction of aqueous solutions of $Fe(NO_3)_3 \cdot 9H_2O$ and As_2O_5. Stoichiometric quantities of each compound were dissolved separately in distilled water, and the two solutions were combined and heated with stirring until the off-white compound precipitated. This precursor product was filtered, washed with distilled water, and dried at 130°C for 2 hr.

Single crystals of $FeAsO_4$ were kindly provided by Professor D'Yvoire of the Laboratoire des Chimie des Solides, C.N.R.S., Université Paris-Sud, Orsay, France.

Polycrystalline $FePO_4$ was prepared by heating stoichiometric amounts of well-ground Fe_2O_3 and $NH_4H_2PO_4$ at 600°C for 8 hr in an alumina crucible, regrinding and heating overnight at 600°C, grinding again and heating for 3 hr at 600°C, and finally regrinding and heating for 5 days in a platinum crucible at 900°C in air. X-ray powder diffraction analysis of the light-brown product showed only the lines of $FePO_4$.

2.2. Crystal Structure Refinement

The crystal structure of $FeAsO_4$ was first determined from neutron powder diffraction data (*9*). The diffraction pattern was indexed according to a monoclinic cell with space group $P2_1/n$ and cell constants a = 7.5636(1), b = 8.0795(1), c = 5.0117(1) Å, β = 104.47(1)°.

TABLE I

SUMMARY OF X-RAY DIFFRACTION DATA FOR $FeAsO_4$

Color	Light brown
Size (mm)	0.008 × 0.092 × 0.200
Crystal system	Monoclinic
Space group	$P2_1/n$ (No. 14)
a (Å)	7.560(1)
b (Å)	8.081(1)
c (Å)	5.012(1)
β (°)	104.42(1)
Temperature (°C)	20
Volume (Å^3)	296.55
Z	4
Formula weight	194.77
Calculated density (g/cm^3)	4.362
μ(Mo) (cm^{-1})	159.55
Diffractometer	Enraf–Nonius CAD4
Radiation (graphite monochromator)	Mo $K\alpha$
Data collected	1900
Max 2θ (°)	60.0
Max h, k, l	10, 11, 7
Data octants	+++, −++, +−+ −−+
Scan method	ω
Absorption correction	Analytical
Transmission factors, range	0.2119–0.7728
$R_{\text{data merge}}$	0.025
No. of unique data ($I > 3.0\sigma(I)$)	609
Refinement method	Full-matrix least squares on F
Anomalous dispersion	As, Fe
Weighting scheme	$\propto[\sigma^2(I) + 0.0009I^2]^{-1/2}$
Atoms refined	Aniso: all
Parameters varied	56
Data/parameter ratio	10.88
R	0.031
R_w	0.032
Error of fit	1.17
Secondary extinc. coeff. (mm)	0.49(1) × 10^{-4}

Single-crystal X-ray diffraction data were collected on an Enraf–Nonius CAD4 diffractometer using the experimental conditions given in Table I. Cell parameters were determined from 25 reflections with $6° < \theta < 23°$. All reflections were corrected for Lorentz and polarization effects, and an analytical absorption correction was applied (*11*). Full-matrix least-squares structural refinements were performed using a series of computer programs developed by J. C. Calabrese (*12*). Starting atomic positions were taken from the neutron powder diffraction study (*9*). A check on the occupancy factors confirmed all sites to be fully occupied. A final difference Fourier showed the strongest peak to be 1.5 e$^-$ located 0.85 Å from As(1). Atomic positional and equivalent isotropic thermal parameters are given in Table II, and anisotropic thermal parameters are shown in Table III.

2.3. Mössbauer Spectroscopy

Approximately 20 mg of the $FeAsO_4$ powder was mixed with an approximately equal weight of boron nitride and packed in a thin nylon (15 mm diam. × 2 mm deep) sample holder. The holder was then mounted in the tail of a flow-type helium-4 cryostat (Janis Research Co., Supervaritemp model). Solid or liquid nitrogen was used as the cryogen for the range 298–48 K, and liquid helium was used for the range 48–1.4 K. The temperature was controlled using a DTC-500 setpoint temperature controller (Lakeshore Cryotronics Co.) connected to an uncalibrated silicon diode and a 10-Ω heater which was mounted on the copper sample block, allowing control to a precision of ±0.01 K or better. A calibrated silicon diode driven by a 10 μA constant current source (Lakeshore Cryotronics) allowed for temperature measurement with an absolute accuracy of about ±0.1 K. In the temperature range between 78 and 48 K, a combination of silicon diode and nitrogen vapor pressure thermometry was used for temperature determination. The Mössbauer spectra were obtained using a conventional constant acceleration spectrometer (Canberra Series 35MCA) in conjunction with a Kr/CO_2 gas proportional counter. The gamma ray source was 75 mC ^{57}Co in a rhodium metal matrix. Curve fitting of the Mössbauer spectra was accomplished using a program written primarily by Stone (*13*) which incorpo-

TABLE II

POSITIONAL[a] AND EQUIVALENT ISOTROPIC THERMAL PARAMETERS[b] FOR $FeAsO_4$

Atom	Site	x	y	z	B_{equiv} (Å^2)
As(1)	4*e*	0.42605(7)	0.70148(7)	1.2769(1)	0.46(3)
Fe(1)	4*e*	0.1751(1)	0.4603(1)	0.7631(1)	0.49(3)
O(1)	4*e*	0.2489(6)	0.6031(5)	1.0750(7)	0.9(1)
O(2)	4*e*	0.4764(5)	0.8739(5)	1.1123(7)	0.8(1)
O(3)	4*e*	0.6080(5)	0.5783(5)	1.3459(8)	0.9(1)
O(4)	4*e*	0.3659(6)	0.7643(5)	1.5610(8)	0.7(1)

[a] Space group $P2_1/n$.
[b] All atoms were refined anisotropically; B_{equiv} is given here.

rates statistical goodness-of-fit and reliability tests.

2.4. *Magnetic Susceptibility*

Magnetic susceptibility measurements for $FeAsO_4$ were made on an S.H.E. Co. SQUID magnetometer/susceptometer at the Francis Bitter National Magnet Laboratory at the Massachusetts Institute of Technology. Susceptibility data were also collected using a standard Faraday balance and a Quantum Design, Inc., SQUID magnetometer at DuPont Central Research.

3. Results

3.1. *Structure*

Important interatomic distances and bond angles for anydrous $FeAsO_4$ are given in Table IV. There are two noteworthy features of this structure: first, it is a network structure in which all of the iron atoms are in a unique five-coordinate environment (Fig. 1), and second, the three-dimensional network is comprised of discrete edge-sharing Fe_2O_8 dimers (Fig. 1) which are bridged by AsO_4 tetrahedra (Fig. 2). This is markedly different from the phosphorus analog, $FePO_4$, which adopts the berlinite ($AlPO_4$) structure with tetrahedrally coordinated cations (*14*). Other examples of five-coordinated trigonal-bipyramidal iron in oxide systems are found in Fe_3PO_7 (*5*) and $Fe_4(PO_4)_2O$ (*6*). The average Fe–O bond length herein, 1.949 Å, compares well with the corresponding length in Fe_3PO_7, 1.968 Å, and the AsO_4 distances (1.679 Å, ave) are in good agreement with previous studies on arsenates. The shortest Fe–Fe distance within

TABLE III

ANISOTROPIC THERMAL PARAMETERS[a] (Å^2) FOR THE ATOMS OF $FeAsO_4$

Atom	B_{11}	B_{22}	B_{33}	B_{12}	B_{13}	B_{23}
As(1)	0.53(2)	0.27(2)	0.54(2)	−0.02(2)	0.06(1)	−0.01(1)
Fe(1)	0.49(3)	0.41(3)	0.57(2)	0.08(2)	0.00(2)	0.02(2)
O(1)	1.1(1)	0.7(1)	0.8(1)	−0.3(1)	0.0(1)	−0.3(1)
O(2)	0.8(1)	0.7(1)	0.9(1)	−0.3(1)	0.0(1)	0.2(1)
O(3)	0.7(1)	0.7(1)	1.4(1)	0.3(1)	0.4(1)	0.3(1)
O(4)	1.1(1)	0.4(1)	0.8(1)	0.01(11)	0.4(1)	−0.3(1)

[a] $\exp[-0.25(B_{11}h^2a^{*2} \ldots + 2(B_{12}hka^*b^* \ldots))]$.

TABLE IV

SELECTED INTERATOMIC DISTANCES (Å) AND ANGLES (°) FOR $FeAsO_4$

As(1)–O(1)	1.666(4)	Fe(1)–O(1)	1.911(4)
As(1)–O(2)	1.710(4)	Fe(1)–O(2)^b	2.014(4)
As(1)–O(3)	1.663(4)	Fe(1)–O(2)^a	2.065(4)
As(1)–O(4)	1.677(3)	Fe(1)–O(3)^c	1.879(4)
		Fe(1)–O(4)^d	1.876(4)
		Fe(1)–Fe(1)^g	3.301(1)
O(1)–As(1)–O(2)	109.8(2)	O(1)–Fe(1)–O(2)^a	158.7(2)
O(1)–As(1)–O(3)	109.8(2)	O(1)–Fe(1)–O(2)^b	86.8(2)
O(1)–As(1)–O(4)	108.3(2)	O(1)–Fe(1)–O(3)^c	103.9(2)
O(2)–As(1)–O(3)	108.4(2)	O(1)–Fe(1)–O(4)^d	100.0(2)
O(2)–As(1)–O(4)	107.6(2)	O(2)^a–Fe(1)–O(2)^b	72.0(2)
O(3)–As(1)–O(4)	112.9(2)	O(2)^a–Fe(1)–O(3)^c	90.3(2)
		O(2)^b–Fe(1)–O(3)^c	128.7(2)
Fe(1)^e–O(2)–Fe(1)^f	108.0(2)	O(2)^a–Fe(1)–O(4)^d	91.4(2)
As(1)–O(2)–Fe(1)^f	126.6(2)	O(2)^b–Fe(1)–O(4)^d	122.9(2)
As(1)–O(2)–Fe(1)^e	125.1(2)	O(3)^c–Fe(1)–O(4)^d	104.8(2)

Note. Symmetry operation codes: $^a\ \frac{1}{2}-x, -\frac{1}{2}+y, \frac{3}{2}-z$; $^b\ -\frac{1}{2}+x, \frac{3}{2}-y, -\frac{1}{2}+z$; $^c\ 1-x, 1-y, 2-z$; $^d\ \frac{1}{2}-x, -\frac{1}{2}+y, \frac{3}{2}-z$; $^e\ \frac{1}{2}-x, \frac{1}{2}+y, \frac{3}{2}-z$; $^f\ \frac{1}{2}+x, \frac{3}{2}-y, \frac{1}{2}+z$; $^g\ -x, 1-y, 1-z$.

the Fe_2O_8 unit is long, 3.30 Å, suggesting that iron–iron repulsion is important. As a result, the contact between the two bridging oxygen atoms (O(2)–O(2) in Fig. 1) is rather short (2.40 Å), and the O(2)–Fe–O(2) bond angle is 72° (Table IV). These bridging oxygen atoms are sp^2 hybridized (the sum of the Fe–O(2)–Fe and Fe–O(2)–As bond angles is 359.7°), and likely assist magnetic exchange coupling between the Fe pairs. Since O(2) bonds to two Fe atoms and one As atom, the As(1)–O(2) bond is somewhat longer than the other As–O bonds. All other oxygen atoms are two-coordinated and bond to one Fe and one As atom. This novel structure therefore presents the possibility of both dimer-confined and three-dimensional (network) magnetic exchange interactions.

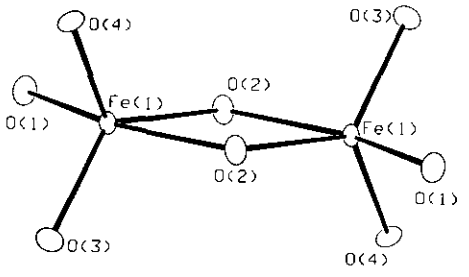

FIG. 1. A dimer of edge-sharing FeO_5 trigonal bipyramids forming an Fe_2O_8 unit in $FeAsO_4$ (*12*).

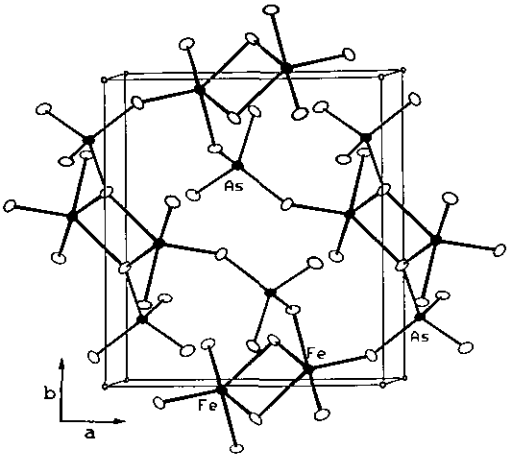

FIG. 2. Interconnected Fe_2O_8 and AsO_4 units in $FeAsO_4$ (*12*).

3.2. *Mössbauer Spectroscopy*

The Mössbauer spectra of $FeAsO_4$ were obtained at temperatures between 298 and

TABLE V

MÖSSBAUER PARAMETERS FOR ANHYDROUS $FeAsO_4$

Temperature (K)	Isomer shift (mm/sec)	Quadrupole splitting (mm/sec)	H_n calcd from $\Delta_{(1-6)}$
29.8	0.291	0.539	0
79.0	0.347	0.547	0
68.9	0.393	0.596	0
65.8			196.6
65.0			245.2
59.3			318.5
55.8			356.7
52.1			385.2
48.5			410.4
40.5			455.7
35.2			475.6
31.1			487.7
26.9			497.6
23.3			503.8
20.1			508.5
17.4			511.0
14.1			514.1
10.6			515.3
4.2			517.2

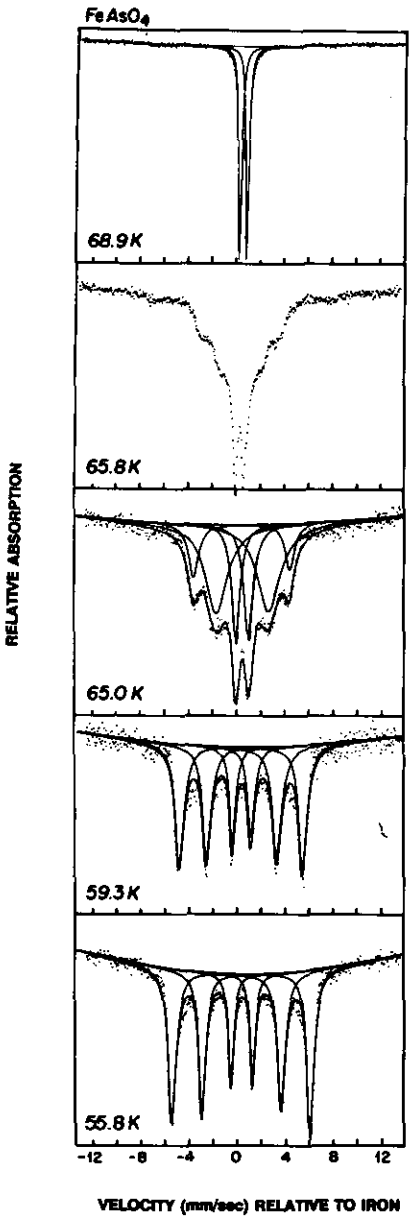

FIG. 3. Mössbauer spectra for $FeAsO_4$ in the temperature range T = 68.9 to 55.8 K.

1.4 K. The results are summarized in Table V and in Figs. 3 and 4. The room temperature spectrum consists of a symmetric quadrupole split doublet (ΔE_Q = 0.54 mm/sec) with isomer shift δ = 0.30 mm/sec. The resolved quadrupole doublet is consistent with the local coordination structure since a distorted five-coordinate high-spin iron site symmetry is expected to give rise to an electric field gradient, which partially removes the degeneracy of the iron ($I = \pm 3/2$) excited nuclear spin state.

Chemical isomer shift values reflect the degree of "*s*" electron density at the nucleus and can, therefore, be related to the *nature and number* of iron–ligand bonds for a given Fe nucleus. For iron, an increase in electron density at the nucleus results in a decrease in chemical shift (*15, 16*) (relative to α-iron). The shift of a tetrahedrally coordinated cation is generally less than that of an octahedrally coordinated cation of the same spin and oxidation state because of the increased covalency of the former (*16*). The tetrahedral four-coordinate Fe(III) of the network solid $FePO_4$, for example, has a room temperature isomer shift of 0.22 mm/sec while the six-coordinate FeO_6 site of $Fe_2(SO_4)_3$, also an Fe(III) network solid, has an isomer shift of 0.49 mm/sec (*1*). The room-temperature isomer shift for the FeO_5 moiety of $FeAsO_4$ is consistent with this coordination number/covalency trend, having a value which lies between that of the four- and six-coordinate complex (FeO_4, FeO_5, and FeO_6 units). The value is close to the room temperature shift for the five-coordinate iron site of Fe_3PO_7, i.e., δ = 0.28 mm/sec, which is itself also consistent with the coordination number/covalency trend. One can rationalize the trend simply in

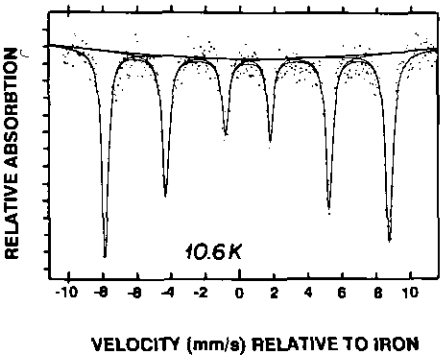

FIG. 4. Mössbauer spectrum for $FeAsO_4$ at T = 10.6 K.

terms of the plausible schemes for tetrahedral high-spin iron (III) (sd^3/sp^3), square-pyramidal five-coordinate (d^2sp^2/sp^3d), and six-coordinate (d^2sp^3/sp^3d^2) in which "s" character decreases as the coordination number increases.

A single quadrupole doublet spectrum is obtained for temperatures down to ~68 K (Fig. 3). At ~67 K, the Mössbauer spectrum begins to broaden and Zeeman split, marking the onset of a transition to three-dimensional magnetic order and the spontaneous development of an internal hyperfine field in zero external field (Figs. 3 and 4). The internal magnetic field continues to increase with decreasing temperature as evidenced by the corresponding increase in the hyperfine splitting of the Mössbauer spectra (Fig. 4). The magnitudes of the internal fields (H_n) were calculated from the overall splitting between transitions 1 and 6, i.e., any quadrupole-shift effects being neglected, for the temperature range 65.8 to 4.2 K (Table V). The rapid onset of magnetic hyperfine field with decreasing temperature is strong evidence for the transition to a three-dimensionally ordered state. The integrated intensity ratios for the six-line hyperfine-split spectra are near 3 : 2 : 1 : 1 : 2 : 3, characteristic of an antiferro- or ferromagnetically ordered thin polycrystalline powder absorber, whose magnetic domains are randomly oriented in zero applied field relative to the direction of gamma ray propagation. The graph of H_n versus T suggests a three-dimensional ordering temperature of $T_{\text{Néel}} = 67 \pm 1$ K.

In view of the resolved quadrupole-splitting observed for $FeAsO_4$ in the paramagnetic phase, i.e., above the ordering temperature, the spectra obtained below the ordering temperature ($T_{\text{Néel}} < \sim 67.5$ K) are presumably the result of a combination of nuclear Zeeman and quadrupole splitting pertubation. For cases such as this, where the Zeeman splitting is larger than the quadrupole interaction, the resulting Mössbauer hyperfine pattern will usually correspond to six transitions except that the center of the inner four transitions is typically shifted toward lower or higher energy relative to the center of transitions 1 and 6. For axial symmetry, this shift may be related to the angle θ between H_n (the internal field and thus the easy axis of magnetization) and the principle axis of the electric field gradient tensor. The relation is given by (*17*)

$$S_1 - S_2 = -\Delta E(3\cos^2\theta - 1),$$

where S_1 is the separation of transitions 1 and 2, S_2 that of transitions 5 and 6, and ΔE is the limiting, low-temperature quadrupole splitting observed for the paramagnetic phase. For this case of combined perturbations, the magnitude of the internal hyperfine field should be calculated from Δ_{2-4} ($=\Delta_{3-5}$) rather than Δ_{1-6}. For purposes of magnetostructural correlations the value for the angle θ is desired since it relates the direction of the internal hyperfine field (and the easy axis) to the principal axis of the electric field gradient tensor where it may be possible to deduce or predict the direction of the latter for sufficiently high symmetry local coordination polyhedra. $S_1 - S_2$ will equal zero (that is, a symmetric spectrum will result) in either of two cases: (1) the trivial case of $\Delta E = 0$, i.e., when there is no quadrupole interaction, or (2) when by coincidence the angle $\theta = \arccos(\sqrt{\frac{1}{3}})$ (i.e., ~54.7°). $S_1 - S_2$ was measured for the hyperfine-split spectra of $FeAsO_4$ and plotted as a function of temperature for the range 59.3 to 4.6 K. Surprisingly, $S_1 - S_2 \sim 0$ (within error) over the entire temperature range which suggests that θ, the angle between H_n and V_{zz} (the principal axis of the electric field gradient tensor) is ~54°. Although this result would seem highly accidental, it is not without precedent. Battle *et al.* (*18*) observed *a nonzero quadrupole interaction in the paramagnetic phase* Mössbauer spectra for the *L*-type ferrimagnet $KBaFe_2(PO_4)_3$ and a *zero quadrupole shift* in the Mössbauer spectrum for the magnetically ordered phase. From this result, the authors concluded that the angle between the principal axis of the electric field

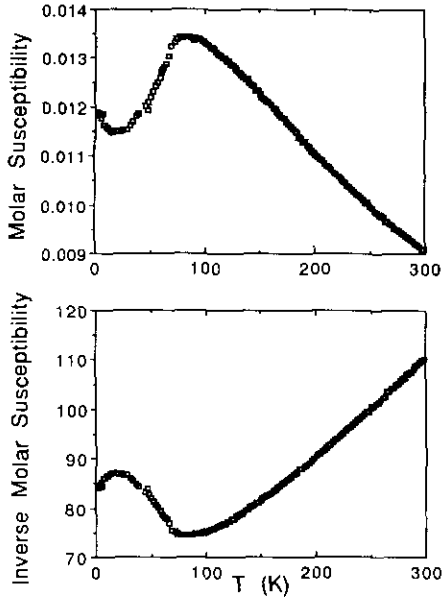

FIG. 5. Molar susceptibility and inverse molar susceptibility obtained by the Faraday method for $FeAsO_4$ with $H_0 = 2$ kG.

gradient tensor and the easy axis of magnetization for the compound in the magnetically ordered state is approximately 54.7° for each of the two nearly equivalent iron sites.

It is worth mentioning here that it is generally possible to obtain more accurate values of the internal field, H_n, from the separations of Δ_{2-4} or Δ_{3-5}. The pairs 2 and 4 or 3 and 5 are due to transitions from the $I = \frac{1}{2}$ ground state terminating in the same M_I sublevel of the $I = \frac{3}{2}$ excited state. Since there is no quadrupole splitting for the $I = \frac{1}{2}$ ground state, the foregoing separations thus lead to the determination of precise values of the Zeeman splitting and, hence, H_n. In the present case, values of H_n calculated from Δ_{1-6} were found equivalent to those calculated from Δ_{2-4} or Δ_{3-5} as expected since there was no apparent quadrupole shift perturbation of the magnetic interaction.

3.3. *Magnetic Susceptibility*

Figure 5 summarizes the results of the magnetic susceptibility study. This figure shows the temperature dependence of the reciprocal susceptibility for $FeAsO_4$. Assuming simple Curie–Weiss law behavior at high temperatures, the linear portion of the curve in the range 190.7 to 291.1 K was extrapolated (via a least-squares linear regression) to the T-axis to obtain Curie constant $C = 4.347$ emu/mol and intercept $\theta = -231$ K. The magnetic moment obtained from the linear region is 5.90 μ_B, in good agreement with the spin-only value of 5.92 μ_B. The large negative paramagnetic Curie temperature is characteristic for a strongly antiferromagnetic material. The temperature dependence of the molar magnetic susceptibility (Faraday balance data determined at DuPont CR&D) of $FeAsO_4$ exhibits a broad maximum at ~84 K, characteristic of a material that exhibits antiferromagnetic exchange interaction. This maximum in susceptibility occurs, however, at a temperature some 17 K higher than the three-dimensional magnetic ordering temperature as determined from the Mössbauer effect experiments ($T_{Néel}$ ~67.5 K). Another interesting feature of the susceptibility versus temperature curve is the evidence of an additional transition which occurs at ~4.5 K (Fig. 6). Essentially identical χ_M versus temperature behavior, including the excursion near 4.5 K and $T_{\chi max}$ ~85 K, was observed for different sample preparations of $FeAsO_4$ in independent susceptibility determinations at Oxford University using a Faraday balance, and a SQUID magnetometer at the National Magnet Lab, M.I.T. A transition occurs in the susceptibility versus temperature curve of $FePO_4$ (*3*) at ~17 K and, as already mentioned, has been correlated with a *spin reorientation* transition in which the spins of the antiferromagnetically ordered material rotate while the structure remains antiferromagnetic. For $FePO_4$, the latter transition also coincided with a systematic, measurable change in the sign and magnitude of the quadrupole shift, S_1–S_2 of the zero-field Mössbauer spectra. However, in repeated measurements, we could observe no evidence of such a feature in our

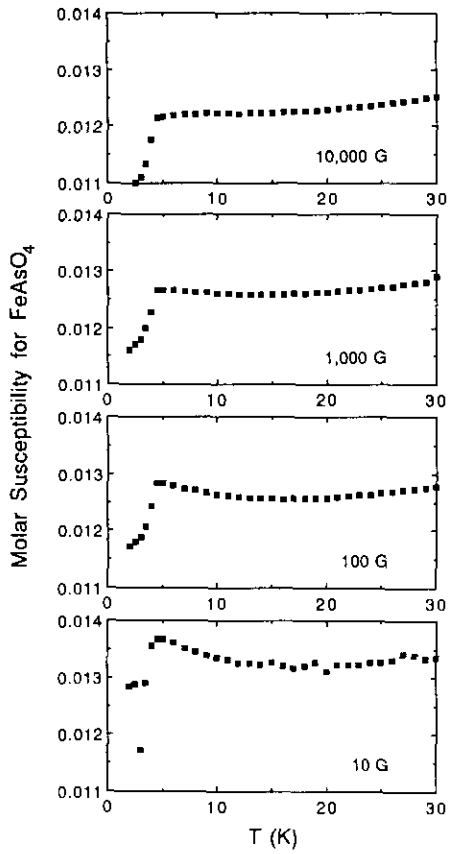

FIG. 6. SQUID magnetometry data for $FeAsO_4$.

S_1–S_2 vs T Mössbauer spectra data for $FeAsO_4$ in the range 20 to 1.39 K. Increasing applied field (H_0) largely suppresses the transition observed at ~4.5 K. We observe complex field dependent behavior in our own comparative study of $FePO_4$, as seen in Fig. 7. In particular, for values of $H_0 <$ 1 kG, χ_M vs T to 2.2 K is relatively featureless save for a broad maximum with an inflection near ~24 K consistent with $T_{Néel} \sim$ 25 K as determined previously via Mössbauer spectroscopy (*19, 20*) and Faraday balance susceptibility studies (*3*) (H_0 = 9.95 kG to ~4.2 K). However, our results show that the spin-reorientation anomaly found at 17 K is not apparent in the magnetic susceptibility data below $H_0 \sim$ 10 kG. Furthermore, a third magnetic transition is now clearly evident at ~5 K for $H_0 >$ 10 kG. (Battle *et al.* (*3*) did not report χ_M vs T to T < 4.2 K.) This system's magnetic behavior is further complicated by the onset of a spin-flop transition for $H_0 \sim$ 15 kG. This is seen in the change in slope of σ vs H for $FePO_4$ (Fig. 8) for 10 kG < H_0 < 20 kG. The latter spin flop is also clear from applied field Mössbauer spectra studies of polycrystalline $FePO_4$ by Bruckner *et al.* (*19*) and Beckmann *et al.* (*20*), wherein a significant fraction of *polycrystalline sample* has already flopped in a longitudinal field of H_0 = 20 kG. (Note that while a spin-flop transition is first order, such a phase change is not expected to be sharp for an initially random polycrystalline sample.) In so far as is possible, random initial states were assured by cooling from ambient temperature to 4.2 K

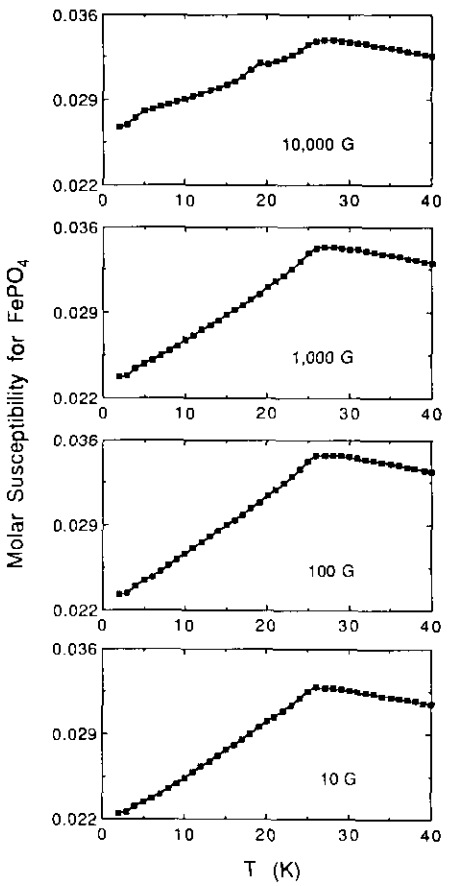

FIG. 7. SQUID magnetometry data for $FePO_4$.

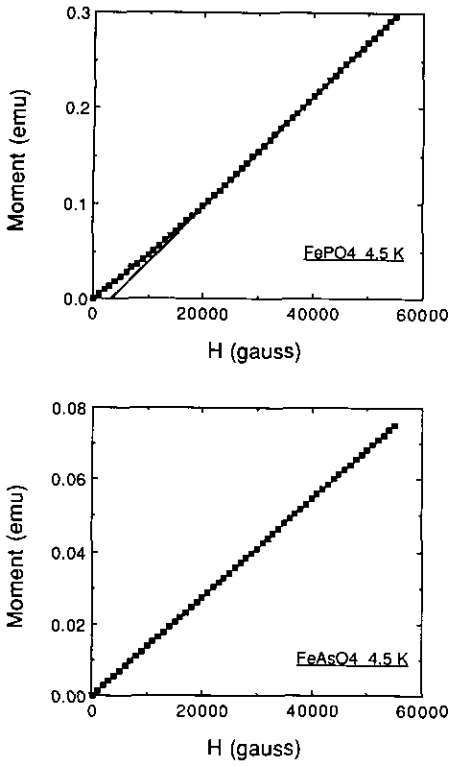

FIG. 8. σ vs H for $FePO_4$ and $FeAsO_4$ at 4.5 K.

in zero applied field. In contrast, σ vs H (Fig. 8) for $FeAsO_4$ is rigorously linear over the range 0 to 60 kG. This implies the absence of any field-induced transitions such as a spin flop. The spin-flop field (H_{SF}) for a uniaxial antiferromagnet is proportional to the product of the exchange (H_E) and anisotropy (H_A) fields as in the relationship: H_{SF} (0° K) = $(2\ H_E H_A - H_A^2)^{1/2}$. In view of the single ion ground states for the ferric species of $FePO_4$ and $FeAsO_4$, i.e., ^6A, corresponding to high-spin Fe(III), H_A should be small and perhaps comparable for these systems. On the other hand, the ratio of the Néel temperatures for these systems is 67.5/24.5 = 2.76, implying a substantially larger value of H_E for the arsenate and correspondingly larger value of H_{SF}. Thus, it is perhaps not surprising that there is no evidence of a spin flop in the σ vs H behavior of $FeAsO_4$.

There are no outstanding features in the χ_M vs T plot corresponding to the presumed 3D magnetic ordering temperature ($T_{Néel}$ ~67 K from Mössbauer results). This observation is not uncommon for magnetically condensed systems that are also exhibiting lower (two or one) dimensional behavior or strong pairwise interactions. However, the inflection point in χ_M vs T is usually taken as $T_{Néel}$ and for the present case corresponds to ~65 K in reasonable agreement with $T_{Néel}$ as determined by the Mössbauer spectroscopy results. The continuous decrease in susceptibility with decreasing temperature, however, strongly suggests dominant antiferromagnetic interactions over the temperature range ~20 K to room temperature.

4. Discussion

Although five-coordination is unusual for high-spin iron (III), it is not unreasonable, since there is no ligand field stabilization energy that would favor say octahedral or tetrahedral stereochemistry. Five-coordination is found among d^0 and d^{10} metal oxides for example, as in $Mg_3(PO_4)_2$ (*21*) and β-$Zn_3(PO_4)_2$ (*22*), for which there is also no ligand field stabilization energy. It is interesting, however, that anhydrous $FeAsO_4$ does not crystallize in the berlinite structure (i.e., alternating FeO_4 and AsO_4 tetrahedra) as is the case for the related phosphorus analog, $FePO_4$. The results of both the Mössbauer spectroscopy and the magnetic susceptibility study of $FeAsO_4$ provide evidence for a transition to a 3D magnetically ordered phase. Owing to the unique structure of $FeAsO_4$, one may intuitively separate the magnetic interactions between the crystallographically equivalent iron sites into two types: inter- and intradimer.

There seems to be little doubt that the broad maximum in the susceptibility versus temperature curve at ~85 K corresponds to the pairwise antiparallel alignment of the iron moments within the Fe_2O_8 dimers. Such a pairwise intradimer interaction cannot produce the large internal magnetic fields necessary to Zeeman split the iron nuclear

spin states and which normally results in the familiar six transition Mössbauer spectrum, since *the ground state of such a dimer* corresponds to $S_{\text{Total Dimer}} = 0$ for $J < 0$. The absence of a hyperfine splitting of the Mössbauer spectra, obtained at temperatures corresponding to the broad maximum in the susceptibility curve, is clearly consistent with the association of this maximum with the antiferromagnetic *dimer interaction*. Hyperfine splitting of the $FeAsO_4$ Mössbauer spectra are not observed until the temperature of the compound is reduced below ~67 K. At this temperature, presumably, the extended interdimer interactions are comparable to the available thermal energy (kT) so that the individual dimers interact giving rise to spontaneous magnetization and long-range magnetic order. Furthermore, since the susceptibility continues to decrease smoothly well below the three-dimensional ordering temperature, antiferromagnetic interdimer coupling is indicated.

Because the bulk magnetism of $FeAsO_4$ appear to be dominated by the antiferromagnetic exchange within the Fe_2O_8 dimeric units, it should be possible to analyze the *high-temperature susceptibility* data as if the compound were comprised of isolated dimers. Based on this assumption, the susceptibility data were analyzed in terms of the familiar Heisenberg–Dirac–Van Vleck dipolar coupling model which relates the magnetic exchange constant J, to magnetic susceptibility for metal dimers. Using this approach for the temperature range 75 K to R.T., the value of J which best fit the experimental χ_M vs temperature data was determined to be $J = -23 \pm 5$ cm^{-1} (i.e., a singlet–triplet separation of $2J \sim 46$ cm^{-1} ($J/k_B = 66.6$ K)), indicating relatively strong antiferromagnetic intradimer exchange. Typical values of J for binuclear iron (III) compounds with Fe–O–Fe angles ~102° are of the order 9 or 10 cm^{-1} as in the dihydroxy bridged [FeL(OH)]$_2$ (*23*) where L is N,N'-ethylenebis(salicylamide) (salen) or [Fe(salen)Cl]$_2$ (*24*), and ~100 cm^{-1} for Fe–O–Fe angles ≥ ~160° as in the monooxobridged iron dimers [Fe(salen)$_2$]O or Fe(salen)$_2$O · py (*25, 26*). The J value for the present system (−23 cm^{-1}) having an Fe–O–Fe bridge angle of ~108°, is consistent with the aforementioned trend of decreasing antiferromagnetic exchange interaction with decreasing linearity of the bridge angle. One is seeing the onset of interdimer interactions in the Mössbauer spectra at ~68 K, i.e., at a temperature comparable to the singlet–triplet separation for the dimer and at which there is still clearly significant population of the paramagnetic $S_{\text{Total}} = 1$ first excited state of the dimers. We emphasize that treating the $FeAsO_4$ magnetic data as if it corresponded to a system of isolated dimers is a crude approximation. The system is structurally a three dimensional network compound. Nevertheless, this approach allows determination of a reasonable estimate for J (intradimer).

To conclude, it is evident from this study that the determination of the temperature and field dependence of powder neutron diffraction is highly desirable for both $FeAsO_4$ and $FePO_4$ even though the latter is not structurally related to the former. This will lead to a clearer understanding of the magnetic transitions, evident in χ_M vs T, and the true nature of the 3D-ordered ground state above and below 4.5 and 17 K, respectively. The complex field dependence of χ_M observed herein clearly suggests the merits of such studies.

Acknowledgments

The authors thank Professor F. d'Yvoire for the crystals of $FeAsO_4$, W. J. Marshall for the single-crystal X-ray data collection, R. S. McLean for the Faraday susceptibility data collection, and D. Groski for the SQUID measurements. Work at Northeastern University is supported by the U.S. National Science Foundation, Division of Materials Research, Solid State Chemistry Program, Grant DMR 8313710, and the Petroleum Research Fund (for funds toward the purchase of a Co^{57} gamma-ray source) under ASC-PRF Grant 2436-AC3. RJBJ thanks S.E.R.C. for a research studentship.

References

1. P. D. Battle, A. K. Cheetham, G. Long, and G. Longworth, *Inorg. Chem.* **21**, 4223 (1982).

2. Z. JIRAK, R. SALMON, L. FOURNES, F. MERRIL, AND P. HAGENMULLER, *Inorg. Chem.* **21,** 4218 (1982).
3. P. D. BATTLE, A. K. CHEETHAM, C. GLEITZER, W. HARRISON, G. J. LONG, AND G. LONGWORTH, *J. Phys. C. Solid State Phys.* **15,** L919 (1982).
4. G. J. LONG, G. LONGWORTH, P. D. BATTLE, A. K. CHEETHAM, R. THUNDATHIL, AND D. BEVERIDGE, *Inorg. Chem.* **18,** 624 (1979).
5. A. MODARESSI, A. COURTOIS, R. GERARDIN, B. MALAMAN, AND C. GLEITZER, *J. Solid State Chem.* **47,** 245 (1983).
6. M. BOUCHDOUG, A. COURTOIS, R. GERARDIN, J. STEINMETZ, AND C. GLEITZER, *J. Solid State Chem.* **42,** 149 (1982).
7. F. J. MORIN, *Phys. Rev.* **78,** 819 (1950).
8. E. C. SHAFER, M. W. SHAFER, AND R. ROY, *Z. Kristallogr.* **108,** 263 (1956).
9. A. K. CHEETHAM, R. J. B. JAKEMAN, W. DAVID, M. M. EDDY, M. W. JOHNSON, AND C. C. TORARDI, *Nature* **320,** 46 (1986).
10. F. D'YVOIRE, *C. R. Hebd. Séanc. Acad. Sci., Paris* **275C,** 949 (1972).
11. J. DE MEULENAER AND H. TOMPA, *Acta Crystallogr.* **19,** 1014 (1965).
12. All X-ray crystallographic calculations were performed on a Digital Equipment Corp. VAX 8800 computer using a system of programs developed by J. C. Calabrese. Structural figures were drawn with the assistance of the ORTEP program, C. K. Johnson (1976).
13. G. M. BANCROFT, A. G. MADDOCK, W. K. OAG, R. H. PRINCE, AND A. J. STONE, *J. Chem. Soc. A,* 1966 (1967).
14. N. M. NG, AND C. CALVO, *Can. J. Chem.* **53,** 2064 (1975).
15. R. S. DRAGO, "Physical Methods in Chemistry", p. 534. W. B. Saunders Co., San Diego (1977).
16. N. N. GREENWOOD, AND T. C. GIBB, "Mössbauer Spectroscopy," p. 240. Chapman and Hall, London (1971).
17. W. M. REIFF, *in* "Proceedings of the NATO Advanced Study Institute on Magneto-Structural Correlation in Exchange Coupled Systems" (R. D. Willett, Ed.), NATO ASI Series C, Vol. 140, pp. 355–388, Reidel, Holland (1985).
18. P. D. BATTLE, A. K. CHEETHAM, W. T. HARRISON, AND G. J. LONG, *J. Solid State Chem.* **62,** 16 (1986).
19. W. BRUCKNER, W. FUCHS, AND G. RITTER, *Phys. Lett.* **26A,** 32 (1967).
20. V. BECKMANN, W. BRUCKNER, W. FUCHS, G. RITTER, AND H. WEGENER, *Phys. Status Solidi* **29,** 2781 (1968).
21. A. G. NORD AND P. KIERKEGAARD, *Acta. Chem. Scand.* **22,** 1466 (1968).
22. J. S. STEVENS AND C. CALVO, *Can. J. Chem.* **45,** 2303 (1967).
23. L. BORER, L. THALKEN, C. CECCARELLI, M. GLICK, J. H. ZHANG, AND W. M. REIFF, *Inorg. Chem.* **23,** 3398 (1984).
24. M. GERLOCH, J. LEWIS, F. E. MABBS, AND A. RICHARDS, *J. Chem. Soc. A,* 112 (1968).
25. J. LEWIS, F. E. MABBS, AND A. RICHARDS, *J. Chem. Soc. A,* 1014 (1967).
26. M. GERLOCH, E. P. MCKENZIE, AND A. D. TOWL, *J. Chem. Soc. A,* 2850 (1969).